Tellus (1995), 47A, 705–721
Printed in Belgium – all rights reserved

TELLUS
ISSN 0280–6495

Dynamical conceptual models of upper-level mobile trough formation: comparison and application

By JOHN W. NIELSEN-GAMMON, *MS 3150, Department of Meteorology, Texas A & M University, College Station, TX 77843-3150, USA*

(Manuscript received 26 August 1994; in final form 20 February 1995)

ABSTRACT

While the formation of upper-level mobile troughs has received little observational attention, a variety of theories have been proposed to explain the genesis and intensification of mobile troughs. For purposes of intercomparison and qualitative application to observed cases, these theories are described in terms of the generation of waves along the tropopause potential vorticity discontinuity. These models are then tested on a case of mobile trough formation which occurred on 19–20 April 1991 and which was poorly forecasted by operational models. The ridge-trough system is found to have been produced primarily by Rossby wave propagation along the tropopause from a newly-developed cutoff cyclone located to the west. Both vertical and horizontal propagation contributed to the development. Another mechanism which appeared to have a positive effect was superposition due to vertical shear and horizontal deformation. A vorticity maximum within the newly-formed trough was amplified and advected southeastward by the developing larger-scale ridge/trough system and later participated in a surface cyclogenesis event.

1. Introduction

Conventional case-study descriptions of observed cyclogenesis commonly begin by discussing a precursor upper-level mobile trough, or "short wave". A problem with this conceptualization of cyclogenesis is that the formation of the upper-level trough and its maintenance until the initiation of cyclogenesis is left unexplained. Subjective and objective synoptic climatologies of upper-level mobile troughs (Sanders, 1988; Lefevre and Nielsen-Gammon, 1995) agree that troughs tend to form well upstream of preferred regions of surface cyclone development. A variety of mechanisms of mobile trough genesis have been proposed, but few comparisons with observed cases have been performed. Two recent observational studies of mobile trough formation over western North America (Sanders, 1988; Orlanski and Sheldon, 1993) use completely different methodologies to arrive at different conclusions, and it is unclear whether the disagreement is due to case-to-case variability or non-overlapping methods.

The purpose of this study is to compare the dynamical mechanisms which have been proposed as possible causes of upper-level mobile trough generation, in the context of a specific case of trough genesis. The different mechanisms are discussed from the common perspective of the amplification waves along the tropopause, in order to emphasize the unique potential vorticity (PV) configurations and processes associated with each mechanism. These concepts are then used to infer the cause of formation of a particular mobile trough which was associated with a poor operational forecast. The distribution and evolution of PV during trough genesis allow qualitative determination of the specific mechanisms contributing to the development. A quantitative diagnosis of the genesis event will be the focus of a subsequent paper.

2. Conceptual model framework: potential vorticity discontinuities

Existing theories of upper-level trough formation involve balanced flow dynamics. Therefore, they are completely describable in terms of the distribution and evolution of the three-dimensional potential vorticity field and associated boundary conditions, such as surface potential temperature (Hoskins et al., 1985). This conceptualization has become increasingly popular for describing extratropical cyclogenesis events, and is similarly useful for describing upper-level mobile troughs.

The background potential vorticity field of upper-level mobile troughs lends itself to the following two simplifications. (1) The upper-level potential vorticity gradient is concentrated at the tropopause. (2) The dynamic tropopause (Danielsen and Hipskind, 1980) is nearly vertical in the vicinity of jet streams.

The first of these simplifications is the motivation for the use of "tropopause maps" (Hoskins and Berrisford, 1988; Davis and Emanuel, 1991; Thorncroft et al., 1993) for representing upper-level potential vorticity. The second has been exploited by Platzman (1949) and Verkley (1994), among others, for understanding waves along jet streams. Together, the above two simplifications allow one to encapsulate the dynamics of the upper troposphere into the motion and influence of a single contour or tightly-packed set of contours, which represent the near-discontinuity of potential vorticity between the troposphere and the stratosphere and which are colocated with the jet stream.

Of particular dynamical importance is the cross-contour component of the flow, for this advective flow "moves" the PV contours, thereby altering the configuration of the balanced winds and temperatures. Regarding the basic state as a straight westerly jet, any departure of the PV contour from its undisturbed position produces a PV anomaly: a region of anomalously high or low values of potential vorticity relative to the basic state or relative to adjacent areas within the same isentropic layer. Associated with these departures of PV from the basic state are variations in wind and temperature which, while strongest near the anomaly, are not confined to the anomaly itself. As discussed in Eliassen and Kleinschmidt (1957), positive PV anomalies (negative PV anomalies in the southern hemisphere), which correspond to equatorward displacements of the PV contour, are associated with a cyclonic circulation, and shall be referred to as troughs. Poleward displacements correspond to ridges. Similar arguments apply to a surface potential temperature gradient (Bretherton, 1966; Thorpe, 1986): high values of potential temperature at the ground, in either hemisphere, imply a cyclonic circulation.

3. Conceptual models of mobile trough generation

Hoskins et al. (1985, §6) uses the paradigm of the previous section to describe Rossby wave propagation and barotropic and baroclinic instability, and argues that the PV perspective leads to "a sharper perception of relationships between the idealized theoretical models and the behaviour of the real atmosphere". Here we use PV concepts to describe and compare theories of mobile trough generation, and in later sections we shall use the same concepts to analyze the formation of an observed mobile trough.

3.1. Modal instability

The first mechanism to be considered is baroclinic instability (Charney, 1947; Eady, 1949), which would produce an upper-level wave and a surface cyclone simultaneously in a form of development which Petterssen called Type A (Petterssen and Smebye, 1971). Baroclinic instability requires opposite-signed gradients of potential vorticity, or its surrogate, at different isentropic levels (Charney and Stern, 1962; Bretherton, 1966). In the atmosphere, this configuration is most often realized by a tropopause PV gradient and a surface potential temperature gradient. With the proper phase shift, the winds associated with a Rossby edge wave along the surface frontal zone can produce PV advections at the level of and partly in phase with the upper-level Rossby wave, so these advections act to amplify the wave. The same phase tilt allows the winds associated with the upper-level Rossby wave to amplify the wave along the surface frontal zone.

Since most cyclones are unambiguously associated with a preexisting upper trough, some investigators have searched for ways that baroclinic instability could lead to a prominent upper-level disturbance with a weaker low-level or surface signal. Recently, Whitaker and Barcilon (1992) considered basic states with weak baroclinicity at low levels and investigated the effects of a shallow stable layer at the surface and enhanced surface friction. Both effects produced the largest wave amplitudes at upper levels, with the upper-level PV gradient interacting either with the weak surface temperature gradient or with a negative PV gradient at the top of the stable layer. Other studies of baroclinic instability with energy concentrated at upper levels have been performed by Snyder and Lindzen (1988) and Staley (1988).

Barotropic instability was proposed by Kuo (1949) as a mechanism for the generation of mobile troughs, although the synoptic example he used is unconvincing. Although barotropic instability is easily distinguished from baroclinic instability on the basis of energetics, the basic mechanism of mutually-reinforcing counter-propagating Rossby waves is the same. A reversal of the PV gradient within a given isentropic layer is required, and the resulting disturbance would be confined to the upper troposphere.

3.2. *Non-modal growth*

Farrell and coworkers have argued against the significance of modal instability in the atmosphere. They observe that the most unstable wavelengths tend to be too large and that a suitable initial disturbance whose spatial structure is allowed to vary is capable of growing much more rapidly than the most unstable mode for a finite period of time. Indeed, the basic-state flow need not be barotropically or baroclinically unstable.

Rivest and Farrell (1992) describe initial conditions which lead to the rapid transient intensification of upper-level mobile troughs. With a two-dimensional, periodic system, they find that optimal growth during a specific period of time is achieved by a combination of cross-gradient PV advection and superposition. Their basic mechanism can be imagined a series of isolated vortices located at upper levels beneath the tropopause and embedded in vertical shear. The winds associated with each vortex are felt at the level of the PV gradient, and the associated advections induce a Rossby wave. If the westward propagation of the induced wave exactly balances the differential advection by the vertical shear, the wave will continue to grow. Meanwhile, if other vortices at lower levels are originally tilted upshear, the differential advection will cause the vortices to become vertically stacked (to "superpose") at some time, and the associated winds and advections at upper levels will amplify as this happens.

The mechanism discussed by Rivest and Farrell is an extension of the conceptually simpler problem of a vortex interacting with a PV gradient. This process can be called the trough-merger mechanism. For example, consider an isolated vortex approaching an upper-level PV gradient from the south. Its associated winds generate a wave along the jet, which grows more and more rapidly as the vortex is drawn closer. An additional interaction not present in the Rivest-Farrell model is that the southerlies associated with the developing wave accelerate the vortex northward toward the jet, allowing even stronger cross-gradient advections but speeding the eventual incorporation of the vortex into the westerlies.

3.3. *Propagation of wave energy*

A somewhat different problem involves a disturbance embedded within a potential vorticity gradient. Additional wave crests and troughs will appear downstream, but not upstream, because of the eastward group velocity of Rossby waves in the upper troposphere (Rossby, 1945). This mechanism was proposed by Yeh (1949) to explain observed wave development downstream of developing cyclones (Cressman, 1948). The group velocity mechanism, as presented, seems to have been directed toward explaining the downstream propagation of long waves, as opposed to mobile troughs, and considerable observational evidence has confirmed that downstream development is common for long waves. Nonetheless, the same dynamical mechanism can in principle produce downstream development of mobile troughs as well.

A closely related theory, explicitly focused on the development of cyclone-scale mobile troughs, has been dubbed downstream baroclinic development, or DBD, by Orlanski and collaborators. Idealized examples are found in Simmons and Hoskins (1979) and Orlanski and Chang (1993), and case studies are reported in Orlanski and Katzfey (1991) and Orlanski and Sheldon (1993). As with the group velocity mechanism, wave energy propagates downstream at upper levels, but the source of the energy is the unstable baroclinic growth of an initial disturbance.

3.4. Superposition

The last mechanism to be considered here involves an increase in circulation due to a reconfiguration of the potential vorticity anomalies, rather than an increase in the magnitudes of the potential vorticity anomalies. For example, Farrell (1989) pointed out that a suitably configured periodic disturbance in a deformation flow can undergo energy growth associated with changes in shape. For a wave on a localized PV gradient, the situation corresponds to an initially small-amplitude wave on an east-west jet which is embedded in diffluence. The diffluence causes the wavelength to decrease while the north-south extent of the wave increases. Although the total area covered by the PV anomalies does not change, the anomalous PV becomes more compact, allowing the circulations associated with the PV to become superimposed and resulting in an increase in the kinetic energy associated with the wave. If the diffluence continues, the wave becomes increasingly elongated in the north-south direction and the kinetic energy weakens. The same sort of mechanism can operate in confluence, in which case the initial disturbance must be elongated in the cross-flow direction.

Another example would be a short-wave, mobile trough entering a long-wave, stationary trough. Initially, the mobile trough may possess little or no positive relative vorticity, since it is embedded within an environment with large-scale negative relative vorticity. As it moves eastward from the large-scale ridge to the large-scale trough, a "digging" jet forms on the west side of the troughs as the PV gradients become superimposed, and the environmental (and total) vorticity in the base of the mobile trough increases. In addition, the winds associated with the large-scale wave preferentially advect the high potential vorticity in the base of the mobile trough southward, further enhancing the strength of the trough. Both processes continue until the mobile trough reaches maximum amplitude at the base of the long-wave trough.

4. Case study selection

On 19–21 April 1991, a mobile trough (hereafter referred to as the "trough", for brevity) formed over the south-central United States, moved to the Atlantic coast, and a vorticity maximum (hereafter "vort max") which formed within the trough triggered a surface cyclone which moved up the East Coast of the United States. The complete absence of a surface cyclone or vort max in the corresponding 48-h forecast of the National Meteorological Center's short range model, the Nested Grid Model (NGM; see DiMego et al., 1992 for a description of the model), attracted attention to this case. Fig. 1 shows the NGM 48-h forecast and verifying analysis for 1200 UTC 21 April 1991 (hereafter, 21/1200). The cyclogenesis event was associated with the analyzed 500 mb vort max (absolute vorticity in excess of $20 \times 10^{-5}\,s^{-1}$) along the East Coast. The vort max was not present in the 48-h forecast, which also underestimated the overall strength of the somewhat larger-scale trough over the eastern United States. In contrast to errors of position, timing, and intensity, modern operational models rarely miss an event completely. The remainder of this paper will focus on two aspects of the initial development at upper levels between 19/0000 and 20/2100: the formation of the East Coast vort max, and the better-forecasted generation of the trough in which the vort max was embedded.

The NGM analysis two days prior, on which the 48-h forecast was based, is shown in Fig. 2. Based upon continuity with later analyses, the incipient vort max would have been located over the southwestern United States, in an area of nearly straight west-to-east upper-level flow. The relative simplicity of the initial upper-level pattern simplifies the interpretation of the dynamical processes, and the fact that the wave developed over a data-rich area allows some degree of confidence to be placed in the analyses. This case was chosen for those reasons, and also because the rapidity of the genesis events would facilitate the analysis and interpretation. The southern United States is not a particularly common or uncommon area for trough genesis (Lefevre and Nielsen-Gammon, 1995), and this particular event is otherwise unremarkable.

The data chosen for the case study are three-hourly analyses from the Mesoscale Analysis and Prediction System, or MAPS (Benjamin et al., 1991). At the time of the event, MAPS analyses were performed in isentropic coordinates from the middle troposphere to the lower stratosphere,

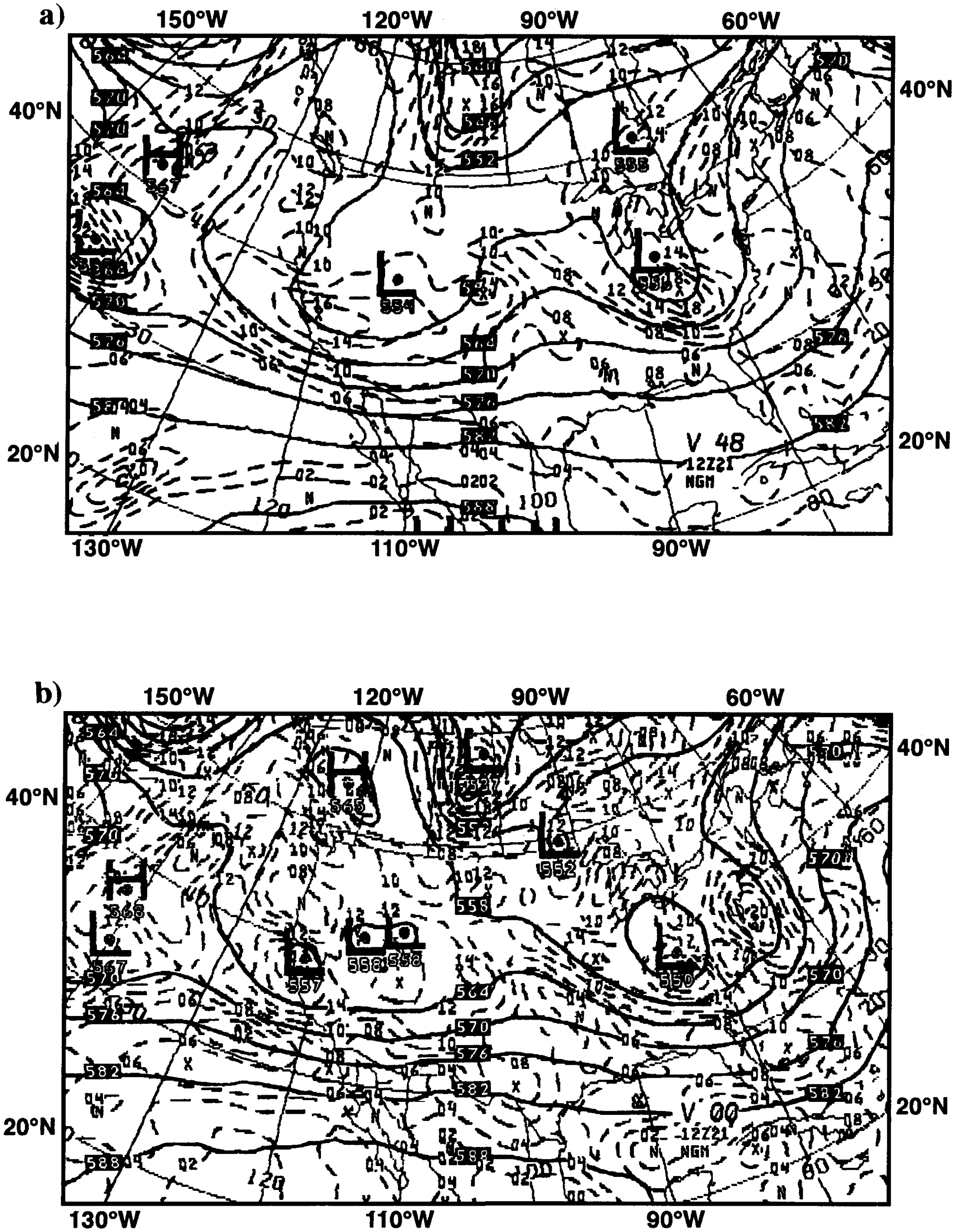

Fig. 1. (a) 48-h 500 mb operational nested grid model (NGM) forecast valid 1200 UTC 21 April 1991, and (b) verifying analysis. Solid contours are geopotential heights, labeled in decameters, and dashed contours are absolute vorticity, labeled in units of 10^{-5} s^{-1}.

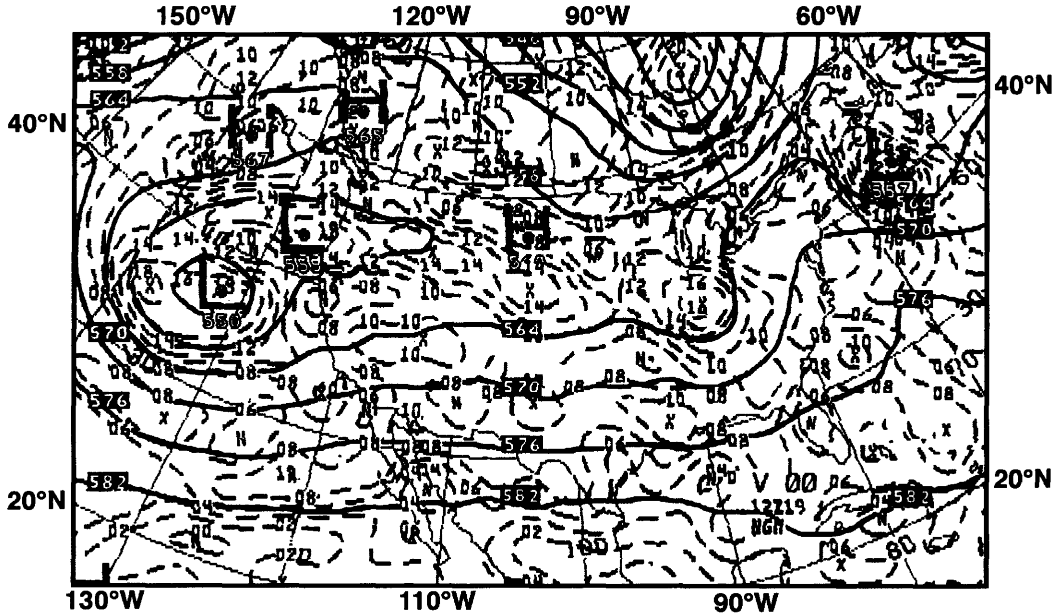

Fig. 2. 500 mb analysis, 1200 UTC 19 April 1991. Solid contours are geopotential heights, labeled in decameters, and dashed contours are absolute vorticity, labeled in units of 10^{-5} s^{-1}.

with a vertical resolution of 6K–8K near the tropopause and a horizontal resolution of about 60 km. The analyses incorporate wind profiler observations and ACARS observations from commercial aircraft. The latter observations are concentrated near the tropopause level, allowing for high temporal and spatial resolution of evolving upper-level features. See Benjamin et al. (1991) for a more complete discussion of observing systems and analysis procedures.

Inspection of consecutive MAPS analyses reveals that the Montgomery streamfunction analyses (and, equivalently, geopotential height analyses on pressure surfaces) show poor continuity, with low centers appearing and disappearing on successive analyses while the winds remain undisturbed. This precludes the use of ageostrophic flux diagnostics (Orlanski and Sheldon, 1993). In contrast, the potential vorticity and wind fields show excellent continuity on a six-hour time scale, and even three-hourly analyses exhibit decent continuity. Problems with the potential vorticity analyses include occasional regions of negative potential vorticity, primarily over the water where analyzable data is scarce, and spuriously high values of potential vorticity when two isentropic surfaces nearly touch. These problems do not seriously constrain this case examination, since the trough formed over a region of the United States with excellent data coverage and our primary interest will be in the regions of strong potential vorticity gradients rather than the magnitudes of maxima and minima. Also, because our interest is in patterns rather than absolute magnitudes, contour labels will be suppressed in the figures which follow.

5. The evolution of the mobile trough

When tracking features at upper-levels, it is conventional to identify and follow the associated 500 mb vorticity maxima. The 3-hourly 500 mb winds (Fig. 3) show the steady development of a moderate-amplitude ridge/trough system from an initially nearly straight zonal flow. The 500 mb vorticity field, however, is dominated by smaller-scale vorticity extrema. The vort max in the base of the mobile trough over Florida and Georgia at 20/2100 (labeled "A") is the same vort max which

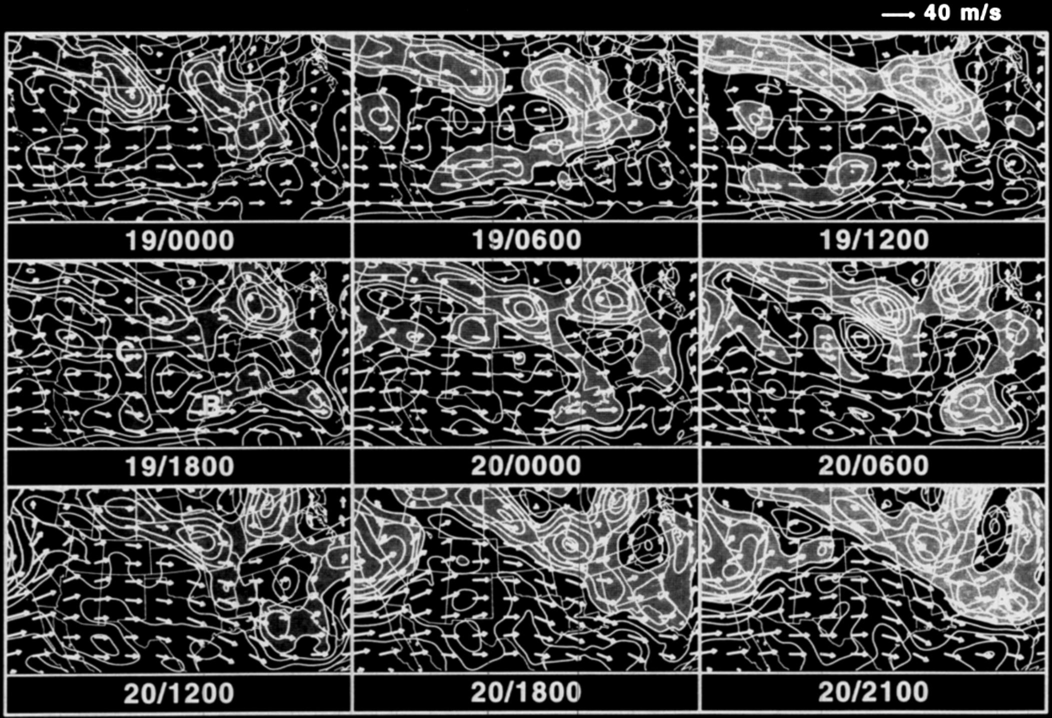

Fig. 3. 500 mb absolute vorticity and winds, from smoothed MAPS analyses. Vorticity is contoured every $2 \times 10^{-5}\ s^{-1}$, with values greater than $1 \times 10^{-4}\ s^{-1}$ shaded. Vector wind scale is as shown.

appears off the East Coast fifteen hours later in Fig. 1b, and is the amalgamation of two preexisting vorticity centers which can be traced back rather erratically to 19/1800. The more southern of the two centers arose from a band of vorticity extending along the Gulf coast ("B"), and the northern center first appeared over Colorado and New Mexico ("C"). Neither maximum underwent rapid intensification; the growth of the trough along the East Coast was associated with a larger-scale increase of vorticity over a wide area of the eastern United States.

At 250 mb (Fig. 4), a different picture emerges. The wind field indicates that the ridge/trough system developed sooner at this level than at 500 mb. In the vorticity field, the vort max over Georgia at 20/2100 ("A") can be traced back as a single region of locally high vorticity to California-Nevada at 19/1200 ("D"). During that 31-hour period, the maximum value of *relative* vorticity more than tripled. This 250 mb vort max was approximately colocated with the northern vorticity center at 500 mb, but the southern 500 mb vorticity center had little or no reflection at the 250 mb level until 20/1200, by which time the two centers had begun to merge. As before, individual vorticity maxima do not provide a complete picture. Note that Fig. 4 shows a concentrated vorticity gradient near the $1.2 \times 10^{-4}\ s^{-1}$ contour, and that this gradient, initially oriented nearly east-west, developed into a high-amplitude wave by 20/1200. It is this change in the vorticity pattern, rather than the intensification of individual vorticity maxima and minima, which is most directly associated with the evolution of the larger-scale trough.

The differing pictures at 250 mb and 500 mb may be reconciled with the help of cross sections (Figs. 5, 6) and isentropic potential vorticity maps (following section). The cross sections are taken in a generally west-east direction through the ridge-trough system (see Fig. 4) and are representative of

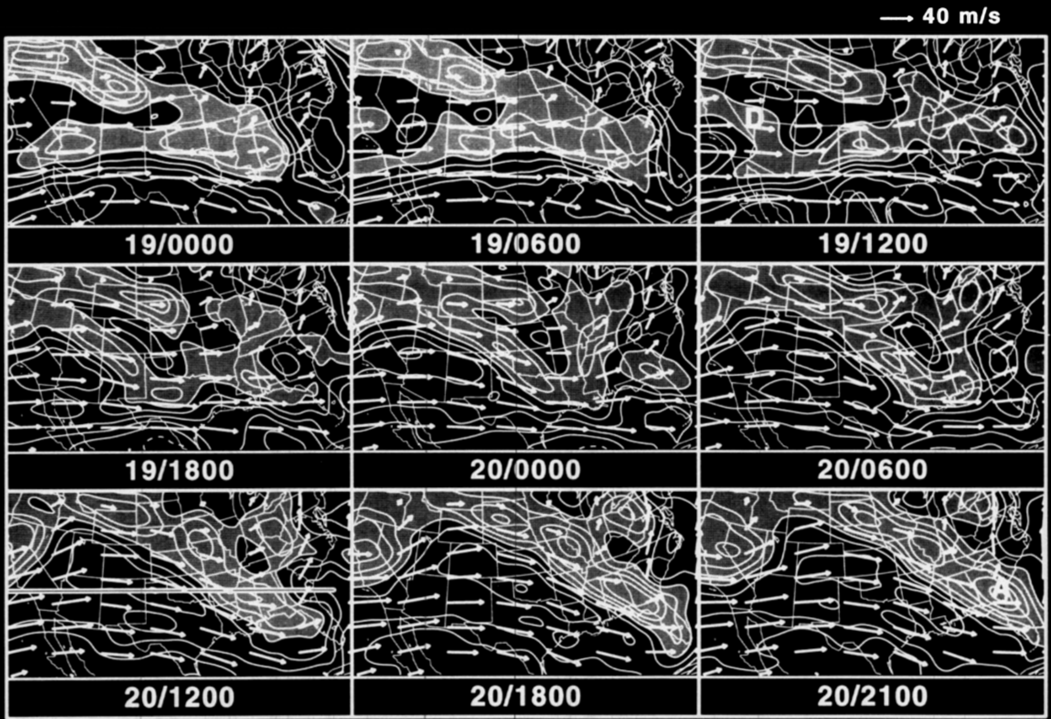

Fig. 4. 250 mb absolute vorticity and winds, from smoothed MAPS analyses. Vorticity is contoured every 3×10^{-5} s^{-1}, with values greater than 1.2×10^{-4} s^{-1} shaded. Vector wind scale is as shown. Horizontal line in lower left panel indicates location of cross sections in Figs. 5, 6.

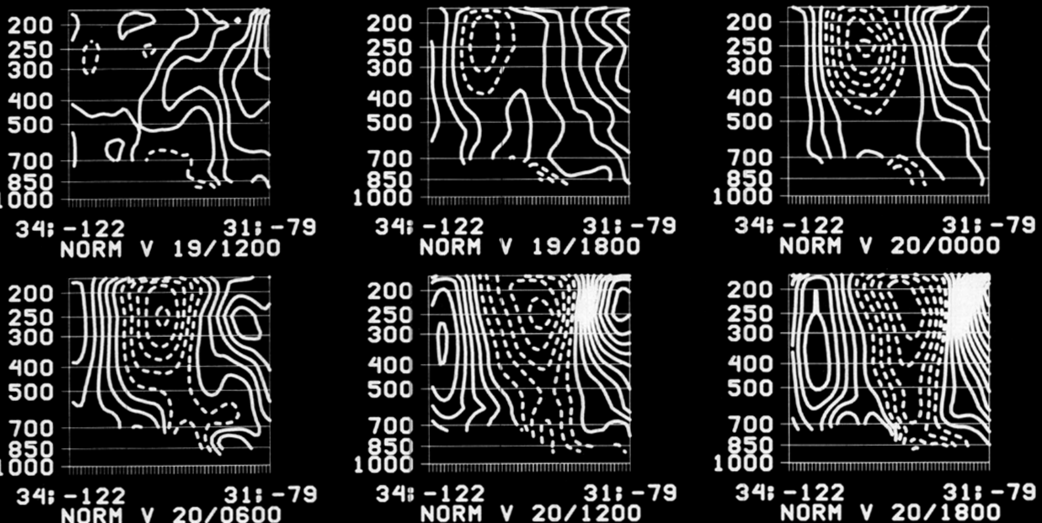

Fig. 5. Vertical sections of the normal component of wind through the developing ridge-trough system. Pressure (mb) is given on the left. Latitude and longitude (negative for °W) of endpoints of cross sections are given at the bottom of each figure. Location of vertical section is shown in Fig. 4. Contour interval is 5 m s^{-1}. Winds out of the page (i.e., from north to south) are dashed.

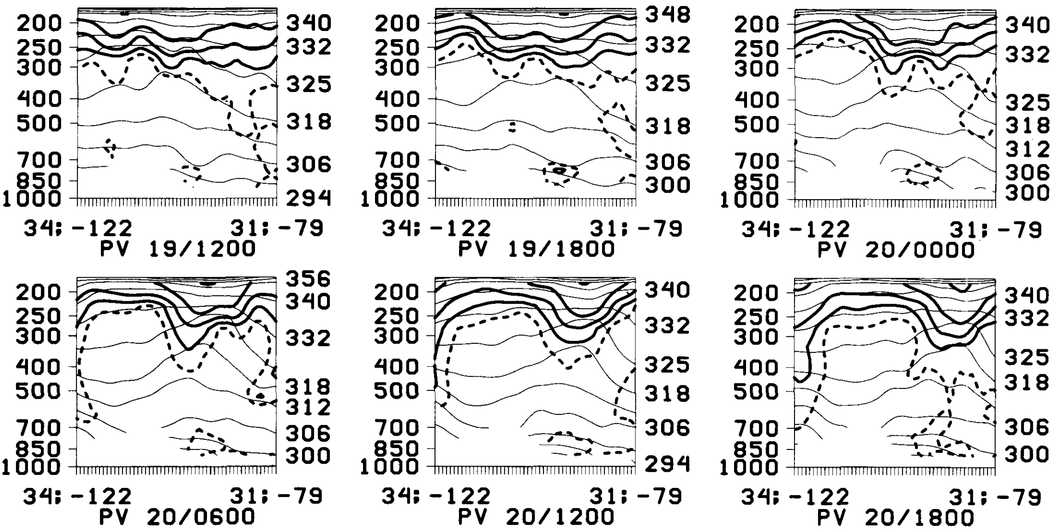

Fig. 6. Vertical sections of potential vorticity and potential temperature through the developing ridge-trough system. Pressure (mb) is given on the left, and potential temperature (K) is given on the right. Potential vorticity contours are at 0.5 (dashed), 1, 2, 4, and 8 PVU; 1 PVU $= 1 \times 10^{-6}$ m^2 K kg^{-1} s^{-1}. Latitude and longitude (negative for °W) of endpoints of cross sections are given at the bottom of each figure. Location of vertical section is shown in Fig. 4.

the vertical structure of the developing system. The development took place initially above 500 mb, as a core of strong northerlies developed between 19/1200 and 20/0000, centered at 250 mb (Fig. 5). The growing trough was associated with a tropopause PV anomaly (Fig. 6) having the classic pattern discussed by Kleinschmidt (1957) and Thorpe (1986). A depressed tropopause, here identified with the 2 PVU surface, was barely present at 19/1200, but the PV anomaly extended to progressively lower isentropic surfaces at later times. By 20/1800, the vertically coherent anomaly extended from the 340–348 K layer to the 318–325 K layer. A core of southerlies had developed downstream by that time, and the winds associated with the developing trough had penetrated downward toward the surface.

Various local PV maxima were present in the lower and middle troposphere. Although not shown in these cross sections, the southern vort max at 500 mb was associated with one such PV anomaly, with a maximum value of PV of about 1 PVU centered near 500 mb. This PV anomaly was not connected to the stratosphere and had the character of an isolated anomaly. As such, although it strongly affected the vorticity distribution at 500 mb, it was not likely to be as significant for cyclogenesis as the developing anomaly at the tropopause, according to the IPV thinking perspective (Hoskins et al., 1985).

(1) Because the anomaly was isolated rather than a wave embedded in a PV gradient, the anomaly could not amplify by cross-gradient advection. This precluded growth by barotropic or baroclinic instability.

(2) Because the anomaly was centered at 500 mb, the "vacuum cleaner effect" (*op. cit.*) could not produce mid-tropospheric vertical motion. This latter point can also be seen through consideration of the vorticity advection term in the quasi-geostrophic omega equation, since the vorticity due to the anomaly would be maximized at 500 mb rather than increasing with height above 500 mb.

The use of 500 mb vorticity maps for qualitative diagnosis of vertical motion and development is based on the implicit assumption that the intensity of vorticity centers is strongest above 500 mb (essentially, at tropopause level). This case appears to be an example in which exclusive use of the 500 mb level for diagnosis and prognosis is inappropriate, for the most important dynamics seem to have taken place at tropopause level, and the development of strong northerlies at 250 mb leads their development at 500 mb by at least twelve hours.

The ridge in the west, as tracked by the $1.2 \times 10^{-4}\ s^{-1}$ absolute vorticity contour at 250 mb, is seen to extend progressively farther north, with the most rapid amplification taking place early in the period. The trough over the southeastern United States, meanwhile, progressively extended farther south, with the most rapid southward movement near the end of the period. The distance between the maximum northward and southward displacements of this contour, a measure of the half-wavelength of the developing wave, increased from 1500 km at 19/1800 to 2700 km at 20/1800. The speed of the wave, computed from the mean speeds of the peak and trough, is $14\ m\ s^{-1}$, which compares to a maximum 250 mb wind speed of greater than $60\ m\ s^{-1}$. The speed of the vort max at 250 mb was $28\ m\ s^{-1}$.

6. Comparison of conceptual models

The vertical structure of the ridge/trough system between 19/1200 and 20/0000 provides evidence against baroclinic instability as a development mechanism. Intensification of the north-south wind only occurs above 500 mb, and almost no tilt is present above that level. However, the most unstable normal mode may have little vertical tilt, especially since large shear is present.

More solid evidence comes from cross sections of potential vorticity, wind, and potential temperature taken across the jet while the wave is growing. Because of the rapid development of the trough, one would expect to find large PV variations if the wave were growing through an instability mechanism. The necessary condition for internal baroclinic or barotropic instability is that the potential vorticity gradient along isentropic surfaces must change sign (Charney and Stern, 1962; Eliassen, 1983). For observed development, one can state a stricter requirement:

Each PV gradient must be sufficiently strong that the wind field associated with a wave along one gradient would be capable of inducing the observed wave amplification along the other gradient.

At a given wavelength, the strength of the associated wind field depends upon the strength of the PV anomaly, and the strength of the anomaly is determined (in the barotropic/baroclinic instability mechanism) by the configuration of the background PV gradient and the magnitude of the cross-gradient flow (the component of flow parallel to the background PV gradient vector). What is meant by a "strong" PV gradient depends on the horizontal scale of the gradient relative to the magnitude of the horizontal displacement of air parcels in the cross-gradient direction within the developing wave. If the PV gradient is relatively concentrated, the magnitude of the PV difference across the gradient determines the strength of an anomaly produced by cross-gradient advection. If the PV gradient is relatively broad, the magnitude of the gradient itself is the determining factor.

In the analyzed cross sections, such as the one shown in Fig. 7, a reversal of the PV gradient along isentropic surfaces is present above 500 mb (near 400 mb between 320 K and 325 K). However, the magnitude of the potential vorticity difference is very small, and it is unlikely that a wave on that gradient could grow to sufficient magnitude to induce the observed amplification at jet stream level. Examination of IPV maps confirmed that no suitably-configured or sufficiently strong perturbation was present along this

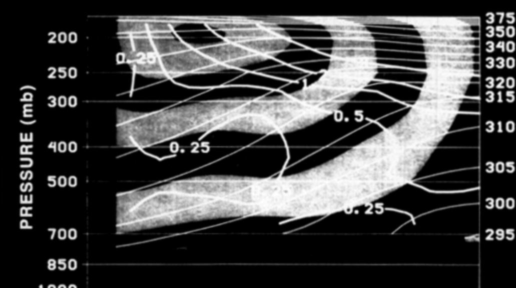

Fig. 7. Representative cross section through the jet along 110° W at the time of initial development of the ridge-trough system. Pressure (mb) is given on the left. Latitude and longitude (negative for ° W) of endpoints of cross sections are given. Alternating bands are the component of wind out of the page (i.e., from west to east); each band is $10\ m\ s^{-1}$ wide, with a maximum value of $62\ m\ s^{-1}$. Thick contours are potential vorticity (PVU; $1\ PVU = 1 \times 10^{-6}\ m^2\ K\ kg^{-1}\ s^{-1}$). Thin contours are potential temperature (K), labels on the right.

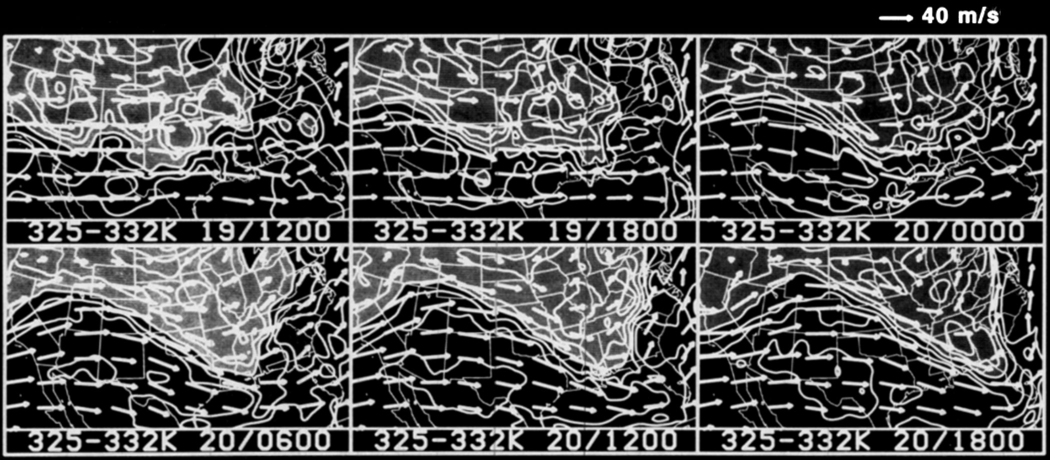

Fig. 8. Mean potential vorticity (PVU) and winds (vector scale given) in the 325–332 K isentropic layer, from unsmoothed MAPS analyses. Potential vorticity is contoured at 0.5, 1, 2, 4, and 8 PVU, with values greater than 2 PVU (nominally, stratospheric air) shaded.

gradient. Therefore, baroclinic and barotropic instability are excluded as possible mechanisms for the development of this mobile trough.

To distinguish among the remaining conceptual models, we first examine the 325–332 K layer, which was the layer with the strongest north-south wind (see Fig. 5) and which was also the layer in which the wave in the PV field developed earliest. Comparison of the PV evolution (Fig. 8) and the 250 mb vorticity evolution (Fig. 4) shows that the cyclonic 250 mb vorticity associated with the short wave tends to lie within and along the edge of the stratospheric PV in the trough, while the anticyclonic vorticity upstream tends to lie within and along the edge of the tropospheric PV in the ridge. As with the 250 mb vorticity field, the amplification of the trough in the 325–332 K layer corresponds to north-south displacements of strong gradients.

Given that the ridge-trough system appears as a wave in the potential vorticity field, the adiabatic and frictionless development of this pattern can only occur through differential advection of PV. Since the potential vorticity contours near the tropopause initially lay roughly east-west, the crucial component of wind is the north-south component. As the ridge/trough system intensifies, the rate of amplification of the pattern should be given by the north-south component of wind in the apex of the ridge or in the base of the trough. In a pure Rossby wave, for example, northerly flow would be expected between the ridge and the downstream trough, but would be exactly zero at the apex of the ridge and the base of the trough. The northerly flow would act to propagate the wave westward, but without change of intensity.

A southerly wind component was present near the western edge of the map at 19/1200. As the ridge developed, this southerly component intensified, reaching 10 m s^{-1} at 19/1800 in the apex of the ridge and remaining strong until after 20/1200. The rate of development of the ridge is consistent with this southerly advection. Downstream, the northerly flow was slower to develop but reached 10 m s^{-1} in the base of the trough by 20/0000 and continued to strengthen after that time. Here too, the rate of intensification of the trough is consistent with this advecting wind. The agreement between the winds and the evolution of PV is a posteriori justification for the assumption that the generation of the ridge/trough system is governed by adiabatic processes. As will be discussed in the following section, this eastward progression of advecting winds suggests Rossby wave propagation or downstream baroclinic development.

A wave developing along a narrow gradient is initially elongated in the along-gradient (in this case, east-west) direction. Deformation can act to intensify the height perturbation associated with the developing wave if the deformation acts to

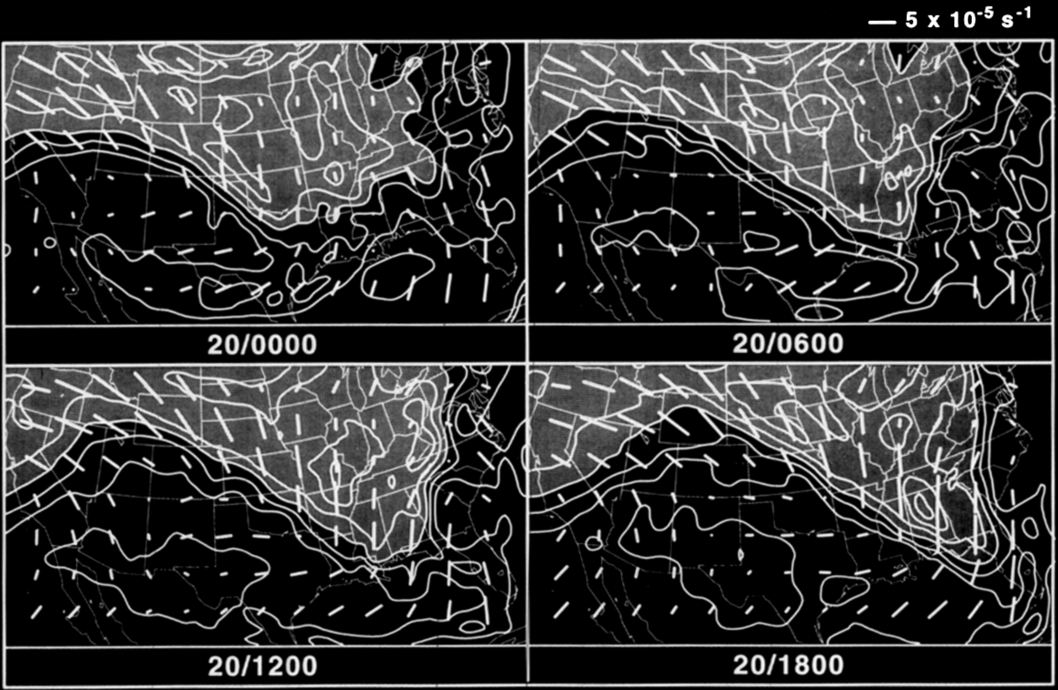

Fig. 9. Mean potential vorticity (PVU) in the 325–332 K isentropic layer from unsmoothed MAPS analyses, and deformation on the 332 K isentropic surface from smoothed MAPS analyses. Potential vorticity is contoured at 0.5, 1, 2, 4, and 8 PVU, with values greater than 2 PVU (nominally, stratospheric air) shaded. Axes of dilatation are drawn as thick lines, with the length of each dilatation axis proportional to the magnitude of deformation (scale as shown).

shrink the along-gradient dimension of the wave. Within the developing ridge, the observed axes of dilatation (Fig. 9) were oriented at a 45° angle to the PV gradient (consistent with shearing deformation), which would neither compact nor elongate the PV anomaly. Downstream, however, the axes of dilatation were oriented north-south throughout the period, which would serve to amplify the height perturbation associated with the developing wave by equalizing the east-west and north-south dimensions of the PV trough. The observed changes in shape of the wave were similar to those expected from the observed deformation: the upstream ridge remained rounded, while the downstream trough developed into a narrow tongue.

Further investigation of the cause of the observed deformation, be it the background large-scale flow, the developing trough itself, or some other mechanism, is beyond the scope of this paper.

The evolving pattern of the north-south component of wind rules out the vortex interaction mechanism for the formation of the trough. If a vortex were approaching the PV gradient at this level, a dipole pattern of north-south wind would have existed, initially separated from the gradient, then increasingly superimposed. Instead, the north-south component of wind developed in situ. The above interpretation is confirmed by charts of PV and the north-south component of wind at this and other isentropic levels (not shown).

A careful comparison of winds and potential vorticity within isentropic layers throughout the troposphere and lower stratosphere is helpful to distinguish from among the remaining possibilities. For brevity, Fig. 10 shows the location of the tropopause potential vorticity gradient within the five isentropic layers which intersect the tropopause in the vicinity of the developing mobile trough. Each band corresponds to the 1–2.5 PVU range within a given isentropic layer, with successively higher layers represented with darker shading.

The width of each band is inversely proportional to the strength of the tropopause PV gradient; a discontinuity would appear as an infinitesimally thin line. A conventional tropopause map, which could be constructed by taking a single PV contour from each layer, is not shown because of the resulting lack of gradient information and the large amount of small-scale variation within the MAPS-analyzed PV fields.

The overall impression of Fig. 10 is of disorder transforming into order. At 19/1200, the PV bands lay in a roughly east-west direction over the western half of the map. By 20/1800, a prominent, coherent wave had developed along each PV gradient, with a ridge to the west and a trough to the east. This development did not take place simultaneously at all levels. The wave first appeared as a ridge in the 325–332 K layer. In time, amplification successively took place within the 332–340 K layer, the 318–325 K layer, the 340–348 K layer, and the 312–318 K layer.

At this point, the Rivest-Farrell mechanism may be eliminated from consideration, since there were no preexisting downshear troughs that would be capable of generating the wave in the 325–332 K layer. On the other hand, superposition may have aided in the intensification of the trough. Recall from Figs. 5, 6 that the tropopause intersected the 325 K surface as early as 19/1200, even though the north-south winds did not become organized until later. The tropopause map provides a possible explanation for the apparent inconsistency. In the 340–348 K layer, a PV ridge was present over the western portion of the map and a PV trough is present over the eastern edge. This pattern persisted throughought the period, with some amplification taking place after 20/0600. At 19/1200, the incipient trough in the 325–332 K layer was colocated with this ridge, while by 20/0600, it is colocated with the downstream trough. Thus, superposition effects would have masked the incipient trough in the height and vorticity field at 19/1200 and enhanced the height response at later times. While this mechanism does not account for the observed growth in amplitude of the PV wave, it can explain a portion of the rapid development of the trough. Part of the superposition process may have involved the larger-

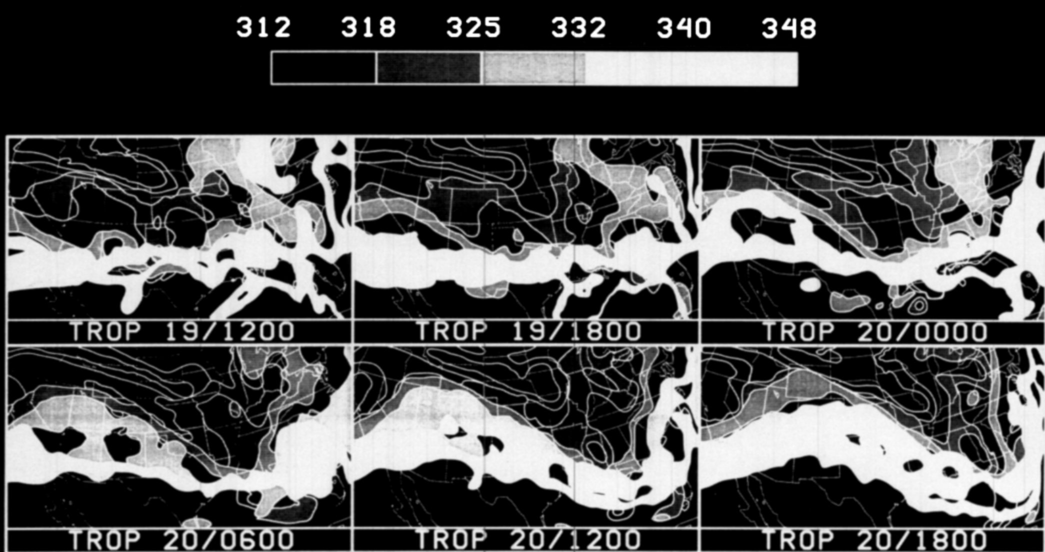

Fig. 10. The position of the tropopause within various isentropic layers. The tropopause is here defined as the 1.0–2.5 PVU potential vorticity band. For each of five isentropic layers, the range of PV values between 1.0–2.5 PVU is shaded, with different shades corresponding to different isentropic layers as given by the table at top. The five shaded bands are then overlaid. The combined maps indicate the isentropic topography of the tropopause, the relative motion of the tropopause within different layers, and the magnitude of the PV gradient at the tropopause.

scale wave at 340–348 K propagating westward against the flow faster than the somewhat smaller trough in the 325–332 K layer.

7. The mechanics of trough formation by downstream energy propagation

Both remaining mechanisms involve downstream propagation of Rossby wave energy. Positive evidence in favor of these mechanisms includes the development of the ridge prior to the development of the trough, suggesting that wave energy entered the region from the west and propagated to the east, and the tendency for the north-south flow amplifying the wave to be strongest along the potential vorticity gradient, suggesting that the PV gradient was acting as a waveguide.

Downstream propagation requires an upstream disturbance. According to Yeh, the disturbance could be any phenomenon which would produce flow across a preexisting potential vorticity gradient. Orlanski and collaborators have given examples of an upstream baroclinic cyclone extracting energy from the large-scale flow. In the present case, an upstream disturbance was present in the form of a newly-developed upper-tropospheric cutoff cyclone (Figs. 1, 2). The cyclone formed off the California coast and was initially quasi-stationary before moving inland near the end of the period. By 20/1800, the cyclone appears in Fig. 10 as a circular region of stratospheric potential vorticity within the 312–318 K layer near the western margin. As seen in vertical sections (Fig. 5), the associated winds did not tilt with height, so the cyclone was barotropic or equivalent-barotropic.

As would be expected, the initial PV ridge-building took place within the isentropic layer (325–332 K) whose strongest PV gradient was located east and southeast of the cutoff cyclone. A gradient farther north could not have been advected far by the cyclonic circulation, while a gradient farther south would have taken longer to come under the influence of the strongest south-to-north advection or any diabatic heating ahead of the cutoff. With time, the PV gradients within both the 325–332 K and 332–340 K layers are brought northward to coincide with the 318–325 K gradient (Fig. 10).

Farther downstream, trough generation can only take place after a ridge has begun forming and northerlies have become established. The trough development will therefore be closely coupled to the upstream ridge development. A specific chain of events is expected: a PV ridge forms, northerlies develop to the east, a PV trough forms to the east, southerlies develop to the east. This pattern can be seen in Figs. 5, 10, and is depicted graphically in Fig. 11. The ridge was weak at 19/1200 and strong at 20/0000; northerlies developed downstream between 19/1500 and 20/0300. There was a hint of a trough at 20/0000 which, as the northerlies strengthened, evolved into a strong trough by 20/1500; southerlies developed downstream during

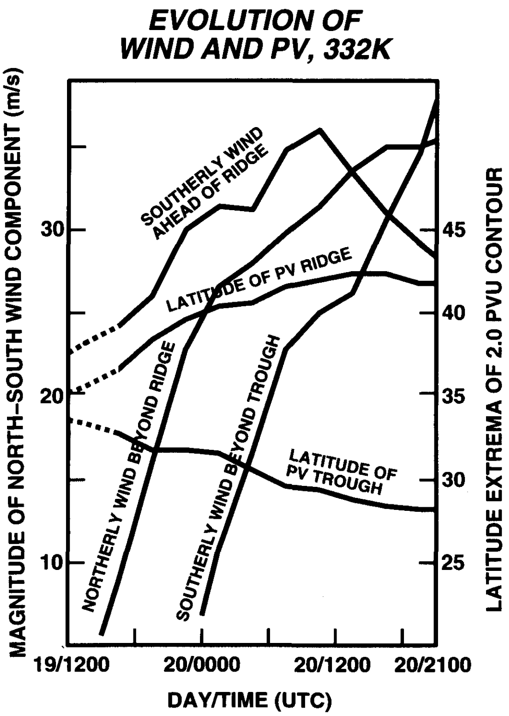

Fig. 11. Evolution of the strength of the north-south wind (black) and amplitude of the ridge-trough system (gray). Winds are maximum southerly wind on the 332 K surface upstream (west) of the developing ridge, average maximum northerly wind between the developing ridge and developing trough, and average maximum southerly wind downstream (east) of the developing trough. Latitudes are average extreme positions of the 2.0 PVU contour within the 325–332 K and 332–340 K layers. All graphs have been passed through a two-point running mean filter.

and after that time. The downstream progression of southerlies and northerlies which takes place along the potential vorticity gradient is strong evidence that the trough was formed by downstream energy propagation.

If the potential vorticity was initially perturbed primarily within the 325–332 K layer, how did a prominent wave develop at all levels between 312 K and 356 K by 20/1800? A suggestion of the answer can be seen in Fig. 10. At 20/0600, the PV troughs at 332–340 K and 318–325 K were nearing the end of their most rapid amplification, which had been brought about by northerly winds downstream of the ridge. The ridge first formed at 325–332, and the northerly flow was strongest in that layer and decreased above and below. In both adjoining layers, particularly in the 318–325 K layer, the PV troughs were upstream of the trough in the 325–332 K layer. This phase shift is consistent with the other troughs being produced by winds associated with the stronger wave in the intermediate layer. This process is essentially Rossby wave propagation.

The details of the process are shown in Fig. 12, which focuses on the propagation to lower isentropic surfaces. The winds in Fig. 12 have had a west-east component of 20 m s^{-1} subtracted from them to better show the cross-gradient advections responsible for amplification. The wind field in the 318–325 K layer closely matched the wind field in the layer above, except that velocities were weaker. The northerly flow was in phase with the developing PV trough at 318–325, allowing rapid amplification of the wave at that level. Essentially, the 318–325 K tropopause had been drawn southward once the wave above it had extended far enough north.

According to simple Rossby wave theory, the 318–325 K PV wave will have an increasingly large effect on the wind field as it amplifies. In particular, it will be directly associated with northerly flow to its west and southerly flow to its east. This flow would be configured to weaken the wave at 325–332 K, thus effecting the transfer of wave energy from one isentropic layer to another. This inhibitory effect from the developing waves at 318–325 K and 332–340 K may be the reason that the PV trough at 325–332 K developed more slowly than the troughs in adjoining layers.

What about the vort max embedded within the trough? A one-to-one association may be made between features on the tropopause map (Fig. 10) and most features in the 250 mb vorticity field (Fig. 4). In particular, the vort max at 250 mb, located over southern Georgia ("A") in the final panel of Fig. 4, is colocated with a nose of high potential vorticity in the 318–325 K layer throughout the evolution. According to Figs. 10, 12, this

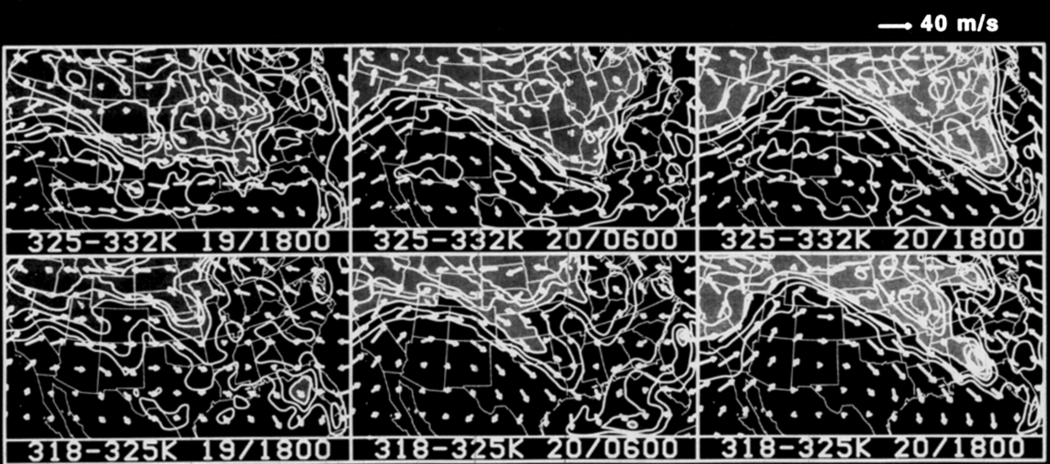

Fig. 12. Mean winds and potential vorticity in the 325–332 K and 318–325 K layers. Potential vorticity is contoured at 0.5, 1, 2, 4, and 8 PVU, with values greater than 2 PVU (nominally, stratospheric air) shaded. Winds are observed winds (scale shown), less a 20 m s^{-1} component from west to east to better show the north-south advection of potential vorticity.

nose of potential vorticity was amplified and drawn into the developing trough by the winds associated with the trough. The amplification was discussed above in the context of vertical Rossby wave propagation, but linear Rossby wave dynamics do not seem to capture the flavor of the event. One might say that the winds associated with the developing larger-scale ridge reached northward, grabbed a tongue of high potential vorticity, and pulled it southward into the trough.

The intensification of the vort max itself may be attributed partly to the intensification of the associated PV anomaly and partly to the motion of the incipient PV anomaly from the ridge axis to the trough axis. The analyses indicate that the magnitude of the PV itself increased within this anomaly; this increase may have been due to inconsistencies within the analyses, or a diabatic mechanism such as the turbulent mixing discussed by Shapiro (1978) may have affected the PV distribution.

8. Summary and discussion

Current theories of upper-level mobile trough generation have been cast in terms of conceptual models based upon a potential vorticity discontinuity at the tropopause. This conceptualization permits a straightforward dynamical comparison of the competing theories. More importantly, it provides a framework for comparing the theories to observed cases of mobile trough generation.

This framework has been applied in a qualitative manner to a specific case of mobile trough formation. The case occurred within the domain of the MAPS isentropic analyses, which provide three-hourly gridded analyses of winds and potential vorticity. The trough was found to have been produced largely by Rossby wave energy propagating eastward along the tropopause PV gradient from a newly-developed upstream cutoff cyclone. The process appears similar to downstream baroclinic development, except that the upstream disturbance does not appear to have been baroclinically growing. Additional elements of the intensification involved superposition due to both vertical shear and horizontal deformation. Barotropic or baroclinic instability did not appear to be operating.

Although the ridge-trough system first formed within a single isentropic layer, the flow associated with the wave quickly allowed the wave to extend itself across isentropic surfaces to other layers. Eventually, the wave became coherent over a depth of 44 K. The eventual development of a coherent PV trough within all five layers by 20/1800 is not predicted by the above cross-isentrope propagation model, and will require further study. Possible reasons for the eventual coherency of the trough include: (1) as the wave propagates along isentropes farther from its source, lines of constant phase should become more vertical; (2) as the wave began interacting baroclinically with the coastal temperature gradient, cyclogenesis became the primary organizing process; (3) vertical wind shear permitted the waves at higher levels to become superimposed; (4) at lower levels, the PV troughs were narrower and were therefore carried downstream more readily by the large-scale west-east flow. This final hypothesis involves a mechanism very similar to what in Section 3 was called digging, with relatively isolated PV anomalies moving from the ridge to the trough of a higher-level wave. In this instance, the digging process involved a finite-amplitude interaction between an incipient vorticity maximum and the developing ridge.

After 20/1200, the vort max triggered a cyclogenesis event along the East Coast of the United States. Neither the vort max nor the cyclogenesis were forecasted to exist by the NGM operational model. Since the upstream cutoff cyclone was present in the initial conditions, poor vertical resolution near the tropopause or a poor analysis of the position of the tropopause may have prevented the model from properly simulating the initial generation of a Rossby wave or the subsequent formation of the vort max.

9. Acknowledgments

This research was funded by the National Science Foundation under grant ATM-9218306. Discussions with Lance Bosart, Haig Iskenderian, and Brian Hoskins were helpful and are very much appreciated, as were the constructive criticisms of two anonymous reviewers.

REFERENCES

Benjamin, S. G., Brewster, K. A., Brummer, R., Jewett, B. F., Schlatter, T. W., Smith, T. L. and Stamus, P. A. 1991. An isentropic three-hourly data assimilation system using ACARS aircraft observations. *Mon. Wea. Rev.* **119**, 888–906.

Bretherton, F. P. 1966. Critical layer instability in baroclinic flows. *Q. J. R. Meteorol. Soc.* **92**, 325–334.

Charney, J. G. 1947. The dynamics of long waves in a baroclinic westerly current. *J. Meteor.* **4**, 135–163.

Charney, J. G. and Stern, M. E. 1962. On the stability of internal baroclinic jets in a rotating atmosphere. *J. Atmos. Sci.* **19**, 159–172.

Cressman, G. P. 1948. On the forecasting of long waves in the upper westerlies. *J. Meteor.* **5**, 44–57.

Danielsen, E. F. and Hipskind, R. S. 1980. Stratospheric-tropospheric exchange at polar latitudes in summer. *J. Geophys. Res.* **85**, 393–400.

Davis, C. A. and Emanuel, K. A. 1991. Potential vorticity diagnostics of cyclogenesis. *Mon. Wea. Rev.* **119**, 1929–1953.

Di Mego, G. J., Mitchell, K. E., Petersen, R. A., Hoke, J. E., Gerrity, J. P., Tuccillo, J. J., Wobus, R. L. and Juang, H.-M. H. 1992. Changes to NMC's regional analysis and forecast system. *Wea. Forecasting* **7**, 185–198.

Eady, E. T. 1949. Long waves and cyclone waves. *Tellus* **1**, 33–52.

Eliassen, A. 1983. The Charney-Stern theorem on barotropic-baroclinic instability. *Pure Appl. Geophys.* **121**, 563–572.

Eliassen, A. and Kleinschmidt, E. 1957. Dynamic meteorology. *Handbuck der Physik* **48**, 1–154.

Farrell, B. F. 1989. Transient development in confluent and diffluent flow. *J. Atmos. Sci.* **46**, 3279–3288.

Hoskins, B. J. and Berrisford, P. 1988. A potential vorticity perspective of the storm of 15–16 October 1987. *Weather* **43**, 122–129.

Hoskins, B. J., McIntyre, M. E. and Robertson, A. W. 1985. On the use and significance of isentropic potential vorticity maps. *Q. J. R. Meteorol. Soc.* **111**, 877–946.

Kuo, H.-L. 1949. Dynamic instability of two-dimensional nondivergent flow in a barotropic atmosphere. *J. Meteor.* **6**, 105–122.

Lefevre, R. J. and Nielsen-Gammon, J. W. 1995. An objective climatology of mobile troughs in the Northern Hemisphere. *Tellus* **47A**, 638–655.

Orlanski, I. and Chang, E. K. M. 1993. Ageostrophic geopotential fluxes in downstream and upstream development of baroclinic waves. *J. Atmos. Sci.* **50**, 212–225.

Orlanski, I. and Katzfey, J. 1991. The life cycle of a cyclone wave in the Southern Hemisphere. Part I: Eddy energy budget. *J. Atmos. Sci.* **48**, 1972–1998.

Orlanski, I. and Sheldon, J. 1993. A case of downstream baroclinic development over western North America. *Mon. Wea. Rev.* **121**, 2929–2950.

Petterssen, S. and Smebye, S. J. 1971. On the development of extratropical cyclones. *Q. J. R. Meteorol. Soc.* **97**, 457–482.

Platzman, G. 1949. The motion of barotropic disturbances in the upper troposphere. *Tellus* **1**, 53–64.

Rivest, C. and Farrell, B. F. 1992. Upper-tropospheric synoptic-scale waves. Part II: Maintenance and excitation of quasi modes. *J. Atmos. Sci.* **49**, 2120–2138.

Rossby, C.-G. 1945. On the propagation of frequencies and energy in certain types of oceanic and atmospheric waves. *J. Meteor.* **2**, 187–204.

Sanders, F. 1988. Life history of mobile troughs in the upper westerlies. *Mon. Wea. Rev.* **118**, 2629–2648.

Shapiro, M. A. 1978. Further evidence of the mesoscale and turbulent structure of upper-level jet stream-frontal zone systems. *Mon. Wea. Rev.* **106**, 1100–1111.

Simmons, A. J. and Hoskins, B. J. 1979. The downstream and upstream development of unstable baroclinic waves. *J. Atmos. Sci.* **36**, 1239–1254.

Snyder, C. and Lindzen, R. S. 1988. Upper-level baroclinic instability. *J. Atmos. Sci.* **45**, 2445–2459.

Staley, D. O. 1988. Baroclinic instability in the upper troposphere. *J. Atmos. Sci.* **45**, 3298–3304.

Thorncroft, C. D., Hoskins, B. J. and McIntyre, M. E. 1993. Two paradigms of baroclinic-wave life cycle behavior. *Q. J. R. Meteorol. Soc.* **119**, 17–55.

Thorpe, A. J. 1986. Synoptic scale disturbances with circular symmetry. *Mon. Wea. Rev.* **114**, 1384–1389.

Verkley, W. T. M. 1994. Tropopause dynamics and planetary waves. *J. Atmos. Sci.* **51**, 509–529.

Whitaker, J. S. and Barcilon, A. 1992. Genesis of mobile troughs in the upper westerlies. *J. Atmos. Sci.* **49**, 2097–2107.

Yeh, T.-C. 1949. On energy dispersion in the atmosphere. *J. Meteor.* **6**, 1–16.